Magnetism of a tetrahedral cluster spin chain

Wolfram Brenig
Institut für Theoretische Physik, Technische Universität Braunschweig, 38106 Braunschweig, Germany

Klaus W. Becker
Institut für Theoretische Physik, Technische Universität Dresden, 01062 Dresden, Germany

(Received 4 May 2001; published 12 November 2001)

We discuss the magnetic properties of a dimerized and completely frustrated tetrahedral spin-1/2 chain. Using a combination of exact diagonalization and bond-operator theory the quantum phase diagram is shown to incorporate a singlet product, a dimer, and a Haldane phase. In addition we consider one- and two-triplet excitations in the dimer phase and evaluate the magnetic Raman cross section which is found to be strongly renormalized by the presence of a two-triplet bound state. The link to a novel tellurate materials is clarified.

DOI: 10.1103/PhysRevB.64.214413 PACS number(s): 75.10.Jm, 75.50.Ee, 75.40.−s, 78.30.−j

I. INTRODUCTION

Low-dimensional quantum magnetism has received considerable interest recently due to the discovery of numerous novel materials with spin-$\frac{1}{2}$ moments arranged in chain, ladder, and depleted planar structures. Many of these materials exhibit unconventional magnetic phases due to dimerization and frustration of antiferromagnetic exchange. Particular effort[1] has been devoted to systems like $SrCu_2(BO_3)_2$,[2,3] which display a complete frustration of the magnetic exchange as in the two-dimensional Shastry-Sutherland model.[4] In one dimension complete frustration can occur in two-leg spin ladders if an additional crosswise exchange is included as depicted in Fig. 1 which resembles a chain of edge sharing tetrahedra. For $J_1=J_3$ such tetrahedral ladders have been investigated in the past.[5–7] Very recently, tellurates of type $Cu_2Te_2O_5X_2$ with $X=$Cl,Br have been identified as a new class of spin-1/2 tetrahedral-cluster compounds.[8] Bulk thermodynamic data have been analyzed in the limit of isolated tetrahedra.[8] Raman spectroscopy, however, indicates a substantial intertetrahedral coupling along the *c*-axis direction of $Cu_2Te_2O_5X_2$.[9] In this direction the exchange topology is likely to be analogous to that of Fig. 1 with $J_1\neq J_3$. From a materials perspective it is an open question if the magnetism of the tellurates can be understood in terms of a dimerized tetrahedral spin ladder. From a theoretical point of view, however, the magnetic properties of this model are an interesting issue which forms the motivation for this work.

The paper is organized as follows. In the remainder of this section we discuss the basic properties of the tetrahedral chain Hamiltonian. In Sec. II the quantum phase diagram is analyzed. In Sec. III a bond-operator method is applied to the tetrahedral chain and in Sec. IV the magnetic Raman cross section is evaluated.

The Hamiltonian of the tetrahedral chain can be written in terms of the total edge-spin operators $\mathbf{T}_{1(2)l}=\mathbf{s}_{1(4)l}+\mathbf{s}_{3(2)l}$ and the dimensionless couplings $b=J_3/J_1$ and $a=J_2/J_1$:

$$\frac{H}{J_1}=\sum_l\left[\mathbf{T}_{1l}\mathbf{T}_{2l}+b\mathbf{T}_{2l}\mathbf{T}_{1l+1}+\frac{a}{2}(\mathbf{T}_{1l}^2+\mathbf{T}_{2l}^2)-\frac{3a}{2}\right]. \quad (1)$$

This model displays infinitely many local conservation laws: $[H,\mathbf{T}_{i(=1,2)l}^2]=0;\ \forall l,i=1,2$. Therefore, the Hilbert space decomposes into sectors of fixed distributions of edge-spin eigenvalues $T_{il}=1$ or 0, each corresponding to a sequences of spin-1 chain segments intermitted by chain segments of *localized* singlets. If $J_1\neq J_3$, the spin-1 chain segments are dimerized. In the infinite-length, dimerized $S=1$ chain sector; i.e., for $T_{il}=1\forall i,l$, the model simplifies to

$$\frac{H}{J_1}=\sum_l\ [\mathbf{S}_{1l}\mathbf{S}_{2l}+b\mathbf{S}_{2l}\mathbf{S}_{1l+1}]+\frac{a}{2}D, \quad (2)$$

where $\mathbf{S}_{il}$ refer to spin-1 operators and D is the number of tetrahedra ("dimers").

The Hilbert space of a single tetrahedron consists of 16 states, i.e., two singlets $\mathcal{S}_{1,2}$, three triplets $\mathcal{T}_{1,2,3}$, and one quintet $\mathcal{Q}$, the energies and T_i quantum numbers of which are listed in Table I. Johnsson and collaborators[8] pointed out that this level scheme implies a singlet to reside within the singlet-triplet gap of the tetrahedron for $1/2<a<2$. Moreover, the ground state switches from $\mathcal{S}_1$ to $\mathcal{S}_2$ at $a=1$, suggesting a line of quantum phase transitions in the (a,b) plane for the lattice model.

II. QUANTUM PHASE DIAGRAM

In this section we discuss the ground state of the tetrahedral chain. To begin, we note that by a shift of one-half of the unit cell, i.e., $\mathbf{T}_{2l(1l+1)}\rightarrow\mathbf{T}_{1l(2l)}$, model (1) is symmetric under the operation $(J_1,a,b)\rightarrow(J_1b,a/b,1/b)$. Therefore, in order to cover the *complete* parameter space for $a,b>0$ it is sufficient to consider the phase diagram in the range of $a\in[0,\infty]$ and $b\in[0,1]$.

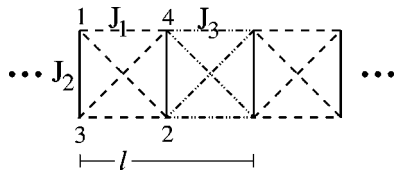

FIG. 1. The tetrahedral cluster chain. l labels the unit cell containing spin-1/2 moments $\mathbf{s}_{i\,l}$ at the vertices $i=1,\ldots,4$.

TABLE I. Eigenstates and energies of the tetrahedron. Columns $T_{1,2}$ refer to corresponding edge-spin quantum number; site index l suppressed.

	T_1	T_2	E/J_1
$\mathcal{S}_1$	1	1	$-2+a/2$
$\mathcal{S}_2$	0	0	$-3a/2$
$\mathcal{T}_1$	1	1	$-1+a/2$
$\mathcal{T}_{2,3}$	0,1	1,0	$-a/2$
$\mathcal{Q}$	1	1	$1+a/2$

Next we note that the ground state of Eq. (1) will be either in the dimerized $S=1$ chain sector or in a homogeneous product of $\mathcal{S}_2$ states only. Inhomogeneous phases consisting of both, $T_{il}=0$ *and* $T_{il}=1$ sites are not allowed for as ground states. To see this we fix b and assume $a\to\infty$, in which case the ground state is a pure product of $\mathcal{S}_2$-type singlets: $|\psi_0\rangle=\Pi_l|\tilde{s}_l\rangle$. Next we check for the ground-state energy change $\Delta E(a,b,N)$ upon forming a single connected chain segment of length N composed out of $T_{il}=1$ sites within the homogeneous state $|\psi_0\rangle$. To be specific we first assume the chain segment to consist of $D'=N/2$ tetrahedra, in which case

$$\Delta E(a,b,D')=D'[2(a-1)-e(b,D')]. \tag{3}$$

Here $-e(b,D')<0$ is the ground-state energy gain *per two sites* due to the intertetrahedral coupling. The main point is that $e(b,D')$ is a monotonously *increasing* function[10] of D'. Therefore the largest critical value $a_c=\max\{a_c(D')\}$ at which the formation of tetrahedra in the $S=1$ sector is favorable, i.e., at which $\Delta E(a_c(D'),b,D')$ turns negative, results for $D'\to\infty$. This implies a single first-order quantum phase transition into the infinite-length, dimerized $S=1$ chain sector as a function of decreasing a. Similar arguments can be pursued for odd N.

In Fig. 2 we show the quantum phase diagram. From Eq. (3) the first-order critical line $a_c(b)$ between the infinite-length, dimerized spin-1 chain for $a<a_c(b)$ and the $\mathcal{S}_2$-type singlet-product state for $a>a_c(b)$ is fixed by $a_c(b)=1+e(b)/2$, where $e(b)=\lim_{D'\to\infty}e(b,D')$. To determine $e(b)$ we have calculated the ground-state energy of dimerized spin-1 chains using exact diagonalization (ED) with periodic boundary conditions (PBC's) on up to $N=16$ sites and a bond-boson theory the results of which will be detailed in Sec. III. Regarding the ED the critical value of $a_c(b=0)=1$ agrees with Ref. 8, while $a_c^{N=16}(b=1)\simeq 1.403$ agrees with Ref. 11 and is consistent with an extrapolated value of $a_c^{N=\infty}(b=1)\simeq 1.401$ from density-matrix renormalization-group (DMRG) calculations[12,7] and ED on 22 sites.[13]

Within the dimerized $S=1$ chain sector an additional second-order quantum phase transition exists between the dimer phase for $b<b_c$ and the Haldane phase for $b>b_c$. This transition has been studied extensively (see, e.g., Ref. 15 and references therein), resulting in $b_c\simeq 3/5$ from DMRG calculations[14] and finite-size scaling analysis.[15] However, this transition is not at the focus of our study. In Fig. 3 our ED results on the finite-size behavior of the spin gap in the dimerized $S=1$ chain sector are shown as function of b, which signals the dimer-Haldane transition and directly reproduces identical data which have been obtained earlier by Kato and Tanaka.[14] Figure 3 contains additional results for the spin gap from the bond-boson approach which we turn to now.

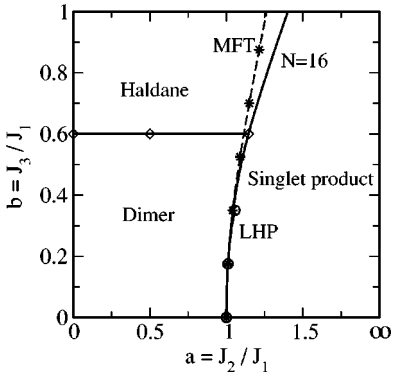

FIG. 2. Quantum phase diagram of the tetrahedral chain. Bare solid line: first-order transition from ED for $N=16$ sites and PBC at 41 values of $b\in[0,1]$. The critical value a_c at $b=1$ from ED is $a_c^{N=16}(b=1)\simeq 1.402\,92$. Solid line with diamond markers: second-order Haldane-dimer transition at $b\simeq 3/5$, extrapolated from ED (see Fig. 3 and Refs. 14 and 15). Dashed (solid) line with starred (circled) markers refers to the bond-boson mean-field, i.e., MFT (Holstein-Primakoff, i.e., LHP) approach. LHP terminates at $b=3/8$.

III. BOND-BOSON ANALYSIS

In this section we detail a mapping of the tetrahedral chain in the dimerized $S=1$ chain sector onto a system of interacting bosons. To this end we adapt the well-developed bond-operator method[16–22] which has proved to be useful in dimerized quantum-spin systems to the present situation. We

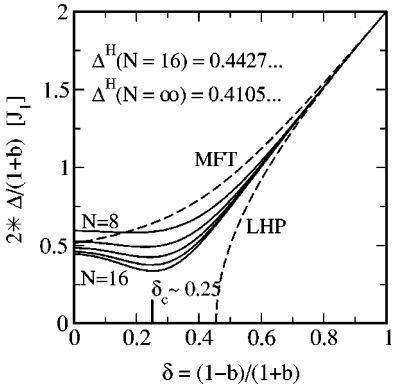

FIG. 3. Solid lines: spin gap Δ from ED for $N=8$, 10, 12, 14, and 16 sites and PBC in the dimerized spin-1 chain sector at 41 values of the intertetrahedral coupling $b\in[0,1]$. Axes have been scaled to allow for a comparison with Ref. 14. Δ^H refers to the spin gap at $b=1$, i.e., the Haldane gap. $\Delta^H(N=16)$ as from this work and $\Delta^H(N=\infty)$ as from Ref. 12. Upper (lower) dashed line: spin gap from bond-boson mean-field, i.e., MFT (Holstein-Primakoff, i.e., LHP) approach.

TABLE II. Bond-boson (BB) representation of the singlet ($\mathcal{S}_1$), triplet ($\mathcal{T}_1$), and quintet ($\mathcal{Q}$) states in the edge-spin $S=1$ sector. $|\rangle$ represents the vacuum. $\hat{\alpha}$ refers to an equivalent running index for each state used to label elements of $M_{\alpha\hat{\beta}\hat{\gamma}}$ and $N_{\alpha\hat{\beta}\hat{\gamma}}$ in Eq. (5). Entries in the ket column refer to S^z eigenstates of $S_{1,2}$ of type $|S_1^z S_2^z\rangle$ with $+,0,-$ denoting $S^z=-1,0,+1$.

	BB	$\hat{\alpha}$	ket
$\mathcal{S}_1$	$s^\dagger\|\rangle$	1	$\frac{1}{\sqrt{3}}(\|-+\rangle+\|+-\rangle-\|00\rangle)$
$\mathcal{T}_1$	$t_x^\dagger\|\rangle$	2	$\frac{1}{2}(\|0+\rangle-\|+0\rangle+\|-0\rangle-\|0-\rangle)$
	$t_y^\dagger\|\rangle$	3	$\frac{i}{2}(\|+0\rangle-\|0+\rangle+\|-0\rangle-\|0-\rangle)$
	$t_z^\dagger\|\rangle$	4	$\frac{1}{\sqrt{2}}(\|+-\rangle-\|-+\rangle)$
$\mathcal{Q}$	$q_2^\dagger\|\rangle$	5	$\|++\rangle$
	$q_1^\dagger\|\rangle$	6	$\frac{1}{\sqrt{2}}(\|+0\rangle+\|0+\rangle)$
	$q_0^\dagger\|\rangle$	7	$\frac{1}{\sqrt{6}}(\|+-\rangle+2\|00\rangle+\|-+\rangle)$
	$q_{-1}^\dagger\|\rangle$	8	$\frac{1}{\sqrt{2}}(\|-0\rangle+\|0-\rangle)$
	$q_{-2}^\dagger\|\rangle$	9	$\|--\rangle$

start by introducing a set of singlet ($s_l^\dagger$), triplet ($t_{l\alpha}^\dagger$), and quintet bosons ($q_{l\alpha}^\dagger$) for each tetrahedron at site l. These bosons create all states within the multiplets $\mathcal{S}_1$, $\mathcal{T}_1$, and $\mathcal{Q}$. The bosons and their corresponding states are listed in Table II. Note that we have chosen an x,y,z (z) representation for the triplet (quintet) states. Moreover, the site index is not displayed in the table.

To suppress unphysical states the bosons have to fulfill the usual hardcore constraint of no double occupancy,

$$s_l^\dagger s_l + t_{l\alpha}^\dagger t_{l\alpha} + q_{l\alpha}^\dagger q_{l\alpha} = 1, \tag{4}$$

where doubly appearing Greek indices are to be summed over their respective ranges. After some straightforward algebra we may express the $\alpha=x,y,z$ components of the edge spins $S_{l1,2}^\alpha$ by

$$S_{l1,2}^\alpha \hat{=} \sqrt{\frac{2}{3}}(\pm s_l^\dagger t_{l\alpha} \pm t_{l\alpha}^\dagger s_l) - \frac{i}{2}\varepsilon_{\alpha\beta\gamma} t_{l\beta}^\dagger t_{l\gamma} \pm M_{\alpha\hat{\beta}\hat{\gamma}} t_{l\hat{\beta}}^\dagger q_{l\hat{\gamma}} \pm M_{\alpha\hat{\beta}\hat{\gamma}}^* q_{l\hat{\gamma}}^\dagger t_{l\hat{\beta}} + N_{\alpha\hat{\beta}\hat{\gamma}} q_{l\hat{\beta}}^\dagger q_{l\hat{\gamma}}. \tag{5}$$

Since $M_{\alpha\hat{\beta}\hat{\gamma}}$ and $N_{\alpha\hat{\beta}\hat{\gamma}}$ will remain unused in the remainder of this work, we defer an explicit display of these quantities to the Appendix. Inserting Eq. (5) into Eq. (2) we arrive at the Hamiltonian

$$H_{BB} = \frac{a}{2}D + H_0 + H_1 + H_2 + H_3 + H_4 + \sum_l \lambda_l (s_l^\dagger s_l + t_{l\alpha}^\dagger t_{l\alpha} + q_{l\alpha}^\dagger q_{l\alpha} - 1), \tag{6}$$

$$H_0 = \sum_l (-2 s_l^\dagger s_l - t_{l\alpha}^\dagger t_{l\alpha} + q_{l\alpha}^\dagger q_{l\alpha}),$$

$$H_1 = -\frac{2b}{3}\sum_l (t_{l\alpha}^\dagger t_{l+1\alpha} s_{l+1}^\dagger s_l + t_{l\alpha}^\dagger t_{l+1\alpha}^\dagger s_{l+1} s_l + \text{H.c.}),$$

$$H_2 = \frac{b}{\sqrt{6}}\sum_l (i\varepsilon_{\alpha\beta\gamma} t_{l+1\alpha}^\dagger t_{l\beta}^\dagger t_{l\gamma} s_{l+1} + \text{H.c.}),$$

$$H_3 = -\frac{b}{4}\sum_l (t_{l\alpha}^\dagger t_{l+1\alpha}^\dagger t_{l+1\beta} t_{l\beta} - t_{l\alpha}^\dagger t_{l+1\beta}^\dagger t_{l+1\alpha} t_{l\beta}),$$

$$H_4 = O(q^{(\dagger)}),$$

where λ_l is a local Lagrange multiplier to enforce the constraint (4). Here H_4 refers to quartic terms involving at least one quintet and at most one singlet boson. Note that the local Hamiltonian H_0 and the first term $Da/2$ simply reflects the spectrum of the single tetrahedron.

To treat the interacting Bose system (6) approximations have to be made. To this end we first realize that in the limit of weak intertetrahedral coupling, i.e., $b \ll 1$, the singlet bosons will condense[16,18] with $s_l^{(\dagger)} \to s \in \Re$. Focusing on this limit and keeping only terms up to quadratic order in the boson operators and, moreover, replacing the local Lagrange multiplier λ_l by a global one we arrive at the mean-field theory (MFT)

$$H_{MFT} = D\left(-2s^2 + \lambda s^2 - \lambda + \frac{a}{2}\right) + \sum_{l\alpha}(\lambda+1) q_{l\alpha}^\dagger q_{l\alpha} - \frac{1}{2}\sum_{k\alpha}(\lambda - 1) + \frac{1}{2}\sum_{k\alpha} \Psi_{k\alpha}^\dagger \begin{bmatrix} \lambda - 1 + s^2\epsilon_k & s^2\epsilon_k \\ s^2\epsilon_k & \lambda - 1 + s^2\epsilon_k \end{bmatrix} \Psi_{k\alpha}, \tag{7}$$

$$\epsilon_k = -\frac{4}{3} b \cos(k), \tag{8}$$

where D is the number of dimers and k is a momentum vector. $\Psi_{k\alpha}^{(\dagger)}$ is a spinor with $\Psi_{k\alpha}^\dagger = [t_{k\alpha}^\dagger t_{-k\alpha}]$ and $t_{l\alpha}^\dagger = \sum_k e^{-ikl} t_{k\alpha}^\dagger / \sqrt{D}$. The mean-field Hamiltonian can be diagonalized by a Bogoliubov transformation, yielding

$$H_{MFT} = D\left(\frac{3}{2} - 2s^2 + \lambda s^2 - \frac{5}{2}\lambda + \frac{a}{2}\right) + \sum_{l\alpha}(\lambda+1) q_{l\alpha}^\dagger q_{l\alpha} + \sum_{k\alpha} E_k \left(a_{k\alpha}^\dagger a_{k\alpha} + \frac{1}{2}\right), \tag{9}$$

where the threefold-degenerate triplet energy E_k is given by

$$E_k = \sqrt{(\lambda-1)^2\left(1+\frac{s^2}{\lambda-1}2\epsilon_k\right)} \tag{10}$$

and the Bogoliubons $a_{k\alpha}^{(\dagger)}$ result from

$$\Psi_{k\alpha} = \begin{bmatrix} g_k & h_k \\ h_k & g_k \end{bmatrix} \Phi_{k\alpha}, \tag{11}$$

where $\Phi_{k\alpha}^{(\dagger)}$ is a spinor with $\Phi_{k\alpha}^{\dagger}=[a_{k\alpha}^{\dagger}a_{-k\alpha}]$ and $h_k^2=[(1+\epsilon_k)/E_k-1]/2$, and $h_k g_k=-\epsilon_k/(2E_k)$ with $h_k^2-g_k^2=1$. Note that on the quadratic level the quintet is *dispersionless*. Substituting $d=s^2/(\lambda-1)$ the ground-state energy is[23]

$$E_{MFT}^0 = D\left(\frac{3}{2}-2s^2+\lambda s^2-\frac{5}{2}\lambda+\frac{a}{2}\right) + \frac{3}{2}(\lambda-1)\sum_k \sqrt{1+2d\epsilon_k}, \tag{12}$$

where we have used that $\langle a_{k\alpha}^{\dagger}a_{k\alpha}\rangle=\langle q_{k\alpha}^{\dagger}q_{k\alpha}\rangle=0$ in the gapped case at $T=0$. The mean-field order parameters s^2 and λ follow from the saddle-point conditions $\partial E_{MFT}^0/\partial s^2=0$ and $\partial E_{MFT}^0/\partial\lambda=0$ which can be combined to result in

$$\frac{5}{2}-d-\frac{3}{2D}\sum_k \frac{1}{\sqrt{1+2d\epsilon_k}}=0, \tag{13}$$

$$\lambda-2+\frac{3}{2D}\sum_k \frac{\epsilon_k}{\sqrt{1+2d\epsilon_k}}=0, \tag{14}$$

with Eq. (13) independent of λ. Therefore, only the single self-consistency equation (13) has to be solved for d with λ following from direct insertion of d into Eq. (14).

In the limit of vanishing intertetrahedral coupling, i.e., $b=0$, Eqs. (13) and (14) reduce to

$$d=1, \quad \lambda=2\rightarrow s^2=1. \tag{15}$$

This case relates the MFT to the linearized Holstein-Primakoff (LHP) method,[19,20] which has found frequent use in bond-boson approaches to dimerized spin-1/2 systems. Within the LHP the constraint is used to eliminate the singlets on the tetrahedra, i.e., within H_0, by $s_l^{\dagger}s_l=1-t_{l\alpha}^{\dagger}t_{l\alpha}-q_{l\alpha}^{\dagger}q_{l\alpha}$. Moreover, within $H_{1,\ldots,4}$ the singlet condensation is implemented with *unit* strength, i.e., $s_l^{(\dagger)}=1$. Dropping all terms beyond quadratic order in the boson operators we arrive at a Hamiltonian which is exactly identical to Eq. (7) with, however, $\lambda\equiv 2$ and $s^2\equiv 1$. Therefore the LHP is *identical* to the MFT constrained to Eq. (15). *A priori* it is not obvious whether the MFT or the LHP is a more reliable approximation and we will present results obtained from both methods.

In Fig. 2 results for $a_c(b)$ as obtained from Eq. (12) are included for the MFT and LHP approaches. As in our ED analysis of Sec. II, the transition occurs at the level crossing of the ground-state energy $E_{MFT(LHP)}^0\equiv D[-2+a/2-e(b)]$ of the spin-1 chain with that of the $\mathcal{S}_2$-type singlet-product state, i.e., $E_{\psi_0}^0=-3Da/2$, which again leads to $a_c(b)=1+e(b)/2$. From Eq. (12) one may read off that the ground-state energy gain per dimer due to intertetrahedral coupling is $-e(b)=7/2-5\lambda/2+s^2(\lambda-2)+3(\lambda-1)\Sigma_k\sqrt{1+2d\epsilon_k}/(2D)$ within MFT, which reduces to $-e(b)=3(\Sigma_k\sqrt{1+2d\epsilon_k}/D-1)/2$ in the LHP approximation. At the dimer to singlet-product phase boundary the agreement with ED is very good for both LHP and MFT. In principle, the singlet condensate restricts the bond-boson approaches to the dimer phase. In fact, the LHP spin gap closes at $b=3/8$, confining the LHP to $b<3/8<b_c$. The MFT can be continued from the dimer into the Haldane regime, even though the ground-state symmetries are different, yielding a transition line qualitatively still comparable to ED.

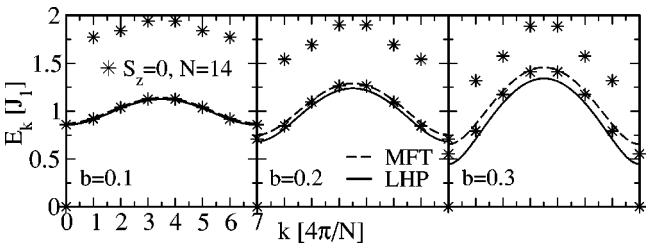

FIG. 4. Dashed (solid) line: E_k as from Eq. (10) for MFT (LHP). Stars: first two total $S_z=0$ excitation of the dimerized spin-1 chain from ED with PBC.

Next we consider elementary excitations of the dimer state. These may (i) remain in the dimerized spin-1 chain sector or (ii) involve transitions into sectors containing *localized* edge singlets, i.e., sites with $T_{il}=0$. In this paper we confine ourselves to the former type. As has been pointed out in Ref. 8, for a single tetrahedron, the energy of a type-(ii) $\mathcal{S}_2$ excitation resides within the spin gap of the type-(i) excitations for $1/2\leqslant a\leqslant 2$. Analogous *dispersionless* singlet gap states occur in the spin gap of the dimer phase of the lattice model and will be discussed elsewhere.[24] Figure 4 compares the dispersion obtained from Eq. (10), for both the MFT and LHP for various values of $b<b_c$, with the first two $S_z=0$ eigenstates obtained from ED on a finite dimerized spin-1 chain with PBC's. Regarding the first triplet excitations the agreement is very good. A comparison of the spin gap, i.e., $E_{k=0,\pi}$, as obtained from the MFT and LHP approaches in the dimerized spin-1 chain sector with ED is contained in Fig. 3. Apart from the fact that the agreement is satisfactory for $b\lesssim 0.2$ this figure demonstrates the main difference between the MFT and LHP approximations. In contrast to the LHP spin gap which closes for $b>3/8$ the MFT overestimates the binding energy due to dimer formation and keeps the spin gap opened for all values of b.

IV. TWO-TRIPLET EXCITATIONS AND RAMAN SCATTERING

Raman scattering can be used to probe the total spin-zero excitations of a spin system at zero momentum. In this section we consider the magnetic Raman scattering in the dimerized $S=1$ sector of the tetrahedral chain. Following

Fleury and Loudon[25] the Raman scattering operator is given by

$$R=\sum_{lm} a_{lm}(\mathbf{E}_i\cdot\mathbf{n}_{lm})(\mathbf{E}_o\cdot\mathbf{n}_{lm})\mathbf{s}_l\cdot\mathbf{s}_m$$

$$=AE_iE_o\sum_l (\mathbf{T}_{l1}\mathbf{T}_{l2}+\beta\mathbf{T}_{l2}\mathbf{T}_{l+11}). \tag{16}$$

$\mathbf{E}_{i(o)}$ are the incoming (outgoing) electric-field vectors and $\mathbf{n}_{lm}$ are unit vectors connecting exchange-coupled sites. a_{lm} are matrix elements which are identical among each of those exchange paths corresponding to one of J_1, J_2, or J_3. From this and the geometry of the tetrahedral chain the second line results for polarizations of the light along the chain—which we will focus on. While β in Eq. (16) will be of order b, it is very unlikely that $\beta=b$. In the latter case the Raman operator commutes with the Hamiltonian, implying a vanishing Raman intensity at nonzero Raman shifts. In the former case we use an equivalent Raman operator

$$\tilde{R}=R-R|_{\beta=b}=C\sum_l \mathbf{T}_{l2}\mathbf{T}_{l+11}, \tag{17}$$

where $C=AE_iE_o(\beta-b)$. Thus the Raman intensity will be of second order in β and b, i.e., the intertetrahedral coupling. To proceed, we approximate $\tilde{R}$ on the level of the LHP:

$$\tilde{R}_{LHP}:=\lim_{q\to 0}\tilde{R}_{LHP}(q)=\lim_{q\to 0}\Bigg[-\frac{2C}{3}\sum_k \cos(k+q/2)$$

$$\times(t^\dagger_{k+q\alpha}+t_{-k-q\alpha})(t^\dagger_{-k\alpha}+t_{k\alpha})\Bigg], \tag{18}$$

where, for later convenience, we have introduced an auxiliary momentum dependence. The Raman intensity can be obtained from the zero-momentum limit of the dynamical susceptibility

$$\chi(q,\tau)=\langle T_\tau[\tilde{R}_{LHP}(q,\tau)\tilde{R}_{LHP}(q,0)]\rangle. \tag{19}$$

Since $\chi(q,\tau)$ is a two-particle propagator, it is important to assess the relevance of two-particle scattering. In particular, it has been realized in the context of other dimerized spin-1/2 systems that magnetic bound states can severely renormalize the bare two-triplet spectrum.[26–29]

We chose to implement the two-particle scattering within the LHP approach. Apart from the interactions $H_{2,\ldots,4}$ in Eq. (6) the constraint (4) implies a hard-core repulsion between two bosons on a site. In the LHP this pertains only to the triplets, as the singlets are condensed and the quintets have been discarded. The hard core is incorporated directly by introducing an additional contribution to the Hamiltonian[26]

$$H_U=U\sum_l t^\dagger_{l\alpha}t^\dagger_{l\beta}t_{l\alpha}t_{l\beta}, \tag{20}$$

with the summation convention on the Greek indices. $\chi(q,\tau)$ is evaluated with H_U at finite U and the limit of $U\to\infty$ is taken at the end.

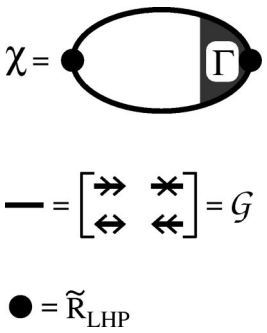

FIG. 5. Raman susceptibility. Thick solid lines label the dressed, 2×2 one-triplet, i.e., $t^{(\dagger)}$-particle matrix Green's functions including diagonal and anomalous contributions. The solid dot refers to the Raman operator (18). Γ is the two-triplet reducible vertex.

The Raman susceptibility corresponds to the diagram depicted in Fig. 5. To simplify matters we focus on the limit $b\ll 1$. In that limit the ground state is nearly a pure product of $\mathcal{S}_1$ singlets and the triplet density induced by quantum fluctuations $n_t=\langle t^\dagger_{l\alpha}t_{l\alpha}\rangle=3\Sigma_k h_k^2$ is a small parameter. As a consequence only the two-triplet *pair*-creation(destruction) vertices contained in Eq. (18) are relevant. Moreover, contributions to the reducible two-particle propagator in Fig. 5 involving anomalous Greens functions, as well as one-triplet self-energy insertions, are suppressed by factors of the triplet density and will be neglected.[26] Physically speaking, the Stokes-Raman process creates two triplets within an approximate singlet-product state. These propagate along the tetrahedral chain and form an interacting two-particle problem with *no* additional triplets generated (destroyed) by quantum fluctuations.[28]

The two-triplet problem allows for an exact solution *including* H_U by the *T*-matrix approach of Fig. 6. This figure depicts the ''particle diagrams,'' which correspond to the Stokes process. For the anti-Stokes process an identical set of ''hole diagrams'' exists with all lines reversed. In the singlet channel only H_3 of Eq. (6) and H_U contribute to the irreducible two-particle vertex γ (see Ref. 30). Due to the momentum space symmetry of γ, it is convenient to formulate the *T*-matrix equation using a 2×2 matrix notation. The bare one-triplet Greens function including normal and anomalous components is given by

$$G^{ij}_\alpha(k,i\omega_n)=\frac{1}{(i\omega_n)^2-E_k^2}\begin{bmatrix} i\omega_n+1+\epsilon_k & -\epsilon_k \\ -\epsilon_k & -i\omega_n+1+\epsilon_k\end{bmatrix}, \tag{21}$$

where ϵ_k and E_k are as of Eqs. (8), (10), and (15), $\alpha=x,y,z$, and $\omega_n=2n\pi T$. $G^{ij}_\alpha(k,i\omega_n)$ satisfies the symmetries $G^{11}_\alpha(k,i\omega_n)=G^{22}_\alpha(k,-i\omega_n)$ and $[G^{21}_\alpha(k,i\omega_n)]^*=G^{21}_\alpha(k,i\omega_n)$. From Fig. 6 we get

$$\chi^p(q,z)=2\chi^0_{cc}+2[\chi^0_{cc}\chi^0_{c1}]\mathbf{V}\left\{\mathbf{1}-\begin{bmatrix}\chi^0_{cc} & \chi^0_{c1}\\ \chi^0_{1c} & \chi^0_{11}\end{bmatrix}\mathbf{V}\right\}^{-1}\begin{bmatrix}\chi^0_{cc}\\ \chi^0_{1c}\end{bmatrix}, \tag{22}$$

where $\chi^0_{cc,c1,1c,11}$ are bare two-particle propagators, the explicit display of whose momentum and frequency depen-

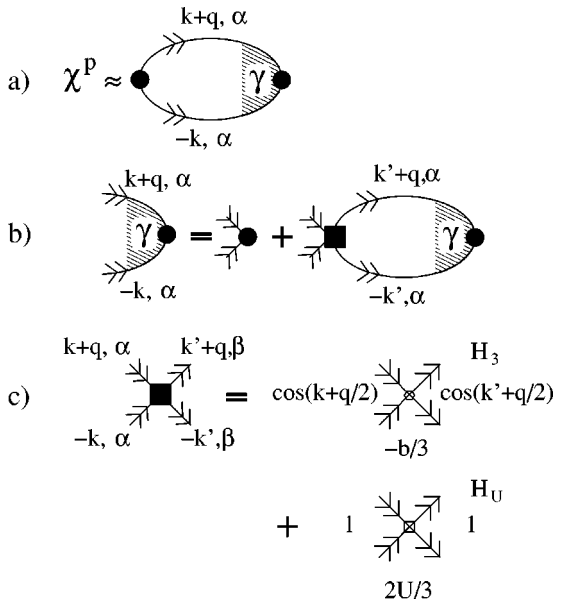

FIG. 6. *T*-matrix approximation to Fig. 5: thin, doubly directed lines label 11 elements of the bare one-triplet Green's function (21). The solid dot is the two-triplet part of the Raman vertex (18). Summation on k' and α is implied in all bare triplet bubbles. γ (solid square) refers to the two-triplet (ir)reducible vertex. Analytic expressions for the two irreducible vertices due to H_3 and H_U are displayed *incorporating* all possible leg exchanges.

dence has been suppressed for brevity. **V** incorporates the momentum-independent coupling-constant factors of the two vertices in γ of Fig. 6:

$$\mathbf{V}=\begin{bmatrix} -b/3 & \\ & 2U/3 \end{bmatrix}, \tag{23}$$

$$\chi^0_{11}(q,z)=3\sum_k \frac{1}{z-E_{k+q}-E_k} \overset{b\ll 1}{\simeq} gA,$$

$$\chi^0_{1c}(q,z)=3\sum_k \frac{\cos\left(k+\frac{q}{2}\right)}{z-E_{k+q}-E_k} \overset{b\ll 1}{\simeq} g(1-\nu A),$$

$$\chi^0_{cc}(q,z)=3\sum_k \frac{\cos^2\left(k+\frac{q}{2}\right)}{z-E_{k+q}-E_k} \overset{b\ll 1}{\simeq} -g\nu(1-\nu A), \tag{24}$$

where we have analytically continued $i\omega_n$ into the upper complex plane $i\omega_n \to z$ and have restricted ourselves to the zero-temperature limit. The prefactors of 3 are due to the sum over the triplet index α and $\chi^0_{1c}(q,z)=\chi^0_{c1}(q,z)$. The two-hole propagator χ^h is obtained by reversing the signs of all $E_{(k)k+q}$ in the denominators of Eq. (24). In the limit $b \ll 1$ one may expand the square root in Eq. (10) which allows for analytic expressions for all of the χ^0's in terms of the quantities g, ν, and A:

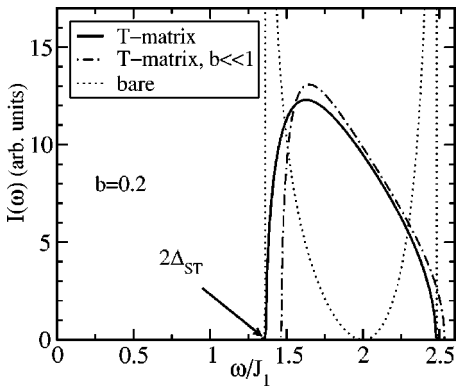

FIG. 7. Raman intensity in the dimer phase at $b=0.2$ as obtained from Eq. (26) (solid), from Eq. (27) dash-dotted, and from Eq. (22) for $\mathbf{V}=0$ (dotted) line. $2\Delta_{ST}$ refers to twice the singlet-triplet gap.

$$g=g(q)=\frac{9}{8b\cos(q/2)}, \quad \nu=\nu(q,z)=\frac{3(z-2)}{8b\cos(q/2)},$$

$$A=A(q,z)=\frac{\mathrm{sgn}[\mathrm{Re}(\nu)]}{\sqrt{\nu^2-1}}. \tag{25}$$

From Eqs. (22)–(25) we obtain the Stokes susceptibility from $\chi^p(q,z)$ by performing the limit $U\to\infty$:

$$\chi^p(q,z)=\frac{6[\chi^0_{11}\chi^0_{cc}-(\chi^0_{1c})^2]}{3\chi^0_{11}+b[\chi^0_{11}\chi^0_{cc}-(\chi^0_{1c})^2]}, \tag{26}$$

$$\overset{b\ll 1}{\simeq} \frac{6\{\mathrm{sgn}[\mathrm{Re}(\nu)]\sqrt{\nu^2-1}-\nu\}}{b\{\mathrm{sgn}[\mathrm{Re}(\nu)]\sqrt{\nu^2-1}-\nu-8\cos(q/2)/3\}}. \tag{27}$$

As in Eq. (22) we refrain from explicitly displaying the momentum and frequency dependence on the right-hand side (RHS) of Eq. (26). From Eqs. (26) and (27) one obtains the Raman intensity $I(\omega)$ from $I(\omega)=-\mathrm{Im}\,\chi^p(0,z\to\omega+i0^+)$ where ω refers to the Raman shift.

Figure 7 shows the Raman intensity contrasting the bare two-triplet spectrum with the interacting one. As is obvious the bare intensity is strongly renormalized by the two-triplet

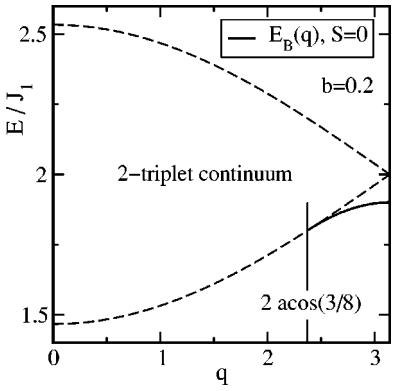

FIG. 8. Two-triplet continuum and dispersion of the $S=0$ bound state from Eq. (27). Note the *y*-axis offset.

TABLE III. Nonzero transition-operator matrix elements [see Eq. (5)] connecting $\mathcal{T}_1$ and $\mathcal{Q}$ as in Table II.

$\hat{\beta}$	$\hat{\gamma}$	$2^{3/2}M_{x\hat{\beta}\hat{\gamma}}$	$\hat{\beta}$	$\hat{\gamma}$	$2^{3/2}M_{y\hat{\beta}\hat{\gamma}}$	$\hat{\beta}$	$\hat{\gamma}$	$2^{3/2}M_{z\hat{\beta}\hat{\gamma}}$
2	5	1	2	5	i			
2	7	$-\sqrt{\frac{2}{3}}$	2	9	$-i$	2	6	-1
2	9	1	3	5	-1	2	8	1
3	5	i	3	7	$-\sqrt{\frac{2}{3}}$	3	6	$-i$
3	9	$-i$	3	9	-1	3	8	$-i$
4	6	-1	4	6	$-i$	4	7	$2\sqrt{\frac{2}{3}}$
4	8	1	4	8	$-i$			

TABLE IV. Nonzero transition-operator matrix elements [see Eq. (5)] within $\mathcal{Q}$ as in Table II.

$\hat{\beta}$	$\hat{\gamma}$	$2N_{x\hat{\beta}\hat{\gamma}}$	$\hat{\beta}$	$\hat{\gamma}$	$2N_{y\hat{\beta}\hat{\gamma}}$	$\hat{\beta}$	$\hat{\gamma}$	$2N_{z\hat{\beta}\hat{\gamma}}$
5	6	1	5	6	$-i$			
6	5	1	6	5	i			
6	7	$\sqrt{\frac{3}{2}}$	6	7	$-i\sqrt{\frac{3}{2}}$	5	5	2
7	6	$\sqrt{\frac{3}{2}}$	7	6	$i\sqrt{\frac{3}{2}}$	6	6	1
7	8	$\sqrt{\frac{3}{2}}$	7	8	$-i\sqrt{\frac{3}{2}}$	8	8	-1
8	7	$\sqrt{\frac{3}{2}}$	8	7	$i\sqrt{\frac{3}{2}}$	9	9	-2
8	9	1	8	9	$-i$			
9	8	1	9	8	i			

interactions. In particular, both of the van Hove singularities present in the bare two-triplet spectrum disappear with the almost symmetric shape of the bare spectrum being deformed by a downward shift of the intensity. These findings allow for a clear physical interpretation which follows from an inspection of the denominators of Eqs. (26) and (27). For $q>q_c$ these denominators acquire a zero for energies $E_B(q)$ below the continuum of the two-triplet scattering states. I.e., a total spin-zero *bound state* exists in the dimerized spin-1 chain at finite momentum.[31] Figure 8 shows the dispersion of this bound state as obtained from Eq. (27) where $q_c = 2a\ \cos(3/8)$. For $q<q_c$ the bound state turns into a resonance shortly above the lower edge of the continuum which leads to the asymmetric Raman intensity of Fig. 7 at $q=0$. This resonance feature has to be contrasted with the impact of bound states on the Raman spectra of other dimerized and frustrated low-dimensional quantum-spin systems where $S=0$ collective modes have been observed rather as sharp excitations *within* the spin gap.[33–35] The actual location of the bound state with respect to the two-triplet continuum is significantly affected by the hard-core repulsion U. Setting $U=0$ in Eq. (22) the short-range attraction due to H_3 would be overestimated with $E_B(q)$ resulting from $1+b\chi^0_{cc}(q,E_B(q))/3=0$ which would yield a bound state *below* the lower edge of the continuum for all q. While $E_B(q)$ in Fig. 8 has been plotted in units of J_1 for $b=0.2$ all bound-state dispersions can be *rescaled* onto a single one in terms of the frequency variable ν. This is certainly an artifact of the limit $b\ll 1$. Finally we note that the relative agreement between Eqs. (26) and (27) improves continuously as $b\to 0$.

V. CONCLUSION

In summary we have investigated the ground state and several aspects of the one- and two-triplet excitations of a tetrahedral cluster spin chain. A number of open questions remain. In particular excitations involving localized edge singlets of the tetrahedra are an issue yet to be resolved. In the case that such excitations are Raman active we expect them to lead to a dispersionless distribution of intensities which can reside in the spin gap of Fig. 7 for certain ranges of the parameters (a,b). Below a temperature of $T\lesssim 50$ K the Raman intensity on $Cu_2Te_2O_5Br_2$ gradually builds up a continuum[9] centered at 60 cm^{-1} which, below $T\lesssim 8$ K, is accompanied by an additional sharp mode developing at 20 cm^{-1}. One might speculate the continuum to correspond to that of Fig. 7 and the sharp mode to consist of transitions involving edge singlets. Yet the measured continuum is rather more symmetric than the solid line in Fig. 7. This might be related to the effects of three-dimensional couplings between the tetrahedra in the tellurates, leaving their magnetism an open issue which deserves further studies. Finally the role of perturbations breaking the complete frustration may be of relevance in the vicinity of the first-order transition leading to additional quantum phases.

ACKNOWLEDGMENTS

The authors are very much indebted to E. Müller-Hartmann for numerous occasions on which he generously shared his many insights into the physics of electron correlations. It is a pleasure to thank P. Lemmens, R. Valenti, C. Gros, F. Mila, E. Kaul, and Ch. Geibel for stimulating discussions and comments. This research was supported in part by the Deutsche Forschungsgemeinschaft under Grant No. BR 1084/1-1 and BR 1084/1-2 and through SFB 463.

APPENDIX: $\mathcal{T}_1\leftrightarrow\mathcal{Q}$ AND $\mathcal{Q}\leftrightarrow\mathcal{Q}$ TRANSITION MATRIX ELEMENTS

In Tables III and IV of this appendix we list the nonzero matrix elements of $M_{\alpha\hat{\beta}\hat{\gamma}}$ and $N_{\alpha\hat{\beta}\hat{\gamma}}$ from Eq. (5). One should note that there are no transitions mediated by $S^{\alpha}_{l1,2}$ between $\mathcal{S}_1$ and $\mathcal{Q}$.

[1] E. Müller-Hartmann, R. R. P. Singh, C. Knetter, and G. S. Uhrig, Phys. Rev. Lett. **84**, 1808 (2000).
[2] H. Kageyama, K. Yoshimura, R. Stern, N. V. Mushnikov, K. Onizuka, M. Kato, K. Kosuge, C. P. Slichter, T. Goto, and Y. Ueda, Phys. Rev. Lett. **82**, 3168 (1999).
[3] S. Miyahara and K. Ueda, Phys. Rev. Lett. **82**, 3701 (1999).
[4] B. S. Shastry and B. Sutherland, Physica B **108**, 1069 (1981).
[5] I. Bose and S. Gayen, Phys. Rev. B **48**, 10 653 (1993).
[6] A. Ghosh and I. Bose, Phys. Rev. B **55**, 3613 (1997).
[7] A. Honecker, F. Mila, and M. Troyer, Eur. Phys. J. B **15**, 227 (2000).
[8] M. Johnsson, K. W. Törnross, F. Mila, and P. Millet, Chem. Mater. **12**, 2853 (2000).
[9] P. Lemmens *et al.*, Phys. Rep. (to be published).
[10] We have checked $e(b,N)$ to increase monotonously with N by evaluating the ground-state energy per site of a dimerized $S=1$ chain with *open* boundary conditions as a function of system size.
[11] T. Sakai and M. Takahashi, Phys. Rev. B **43**, 13 383 (1991).
[12] S. R. White and D. A. Huse, Phys. Rev. B **48**, 3844 (1993).
[13] O. Golinelli, T. Jolicoeur, and R. Lacaze, Phys. Rev. B **50**, 3037 (1994).
[14] Y. Kato and A. Tanaka, J. Phys. Soc. Jpn. **63**, 1277 (1994).
[15] K. Totsuka, Y. Nishiyama, N. Hatano, and M. Suzuki, J. Phys.: Condens. Matter **7**, 4895 (1995).
[16] S. Sachdev and R. N. Bhatt, Phys. Rev. B **41**, 9323 (1990).
[17] A. V. Chubukov and Th. Jolicoeur, Phys. Rev. B **44**, 12 050 (1991).
[18] S. Gopalan, T. M. Rice, and M. Sigrist, Phys. Rev. B **49**, 8901 (1994).
[19] O. A. Starykh, M. E. Zhitomirsky, D. I. Khomskii, R. R. P. Singh, and K. Ueda, Phys. Rev. Lett. **77**, 2558 (1996).
[20] R. Eder, Phys. Rev. B **57**, 12 832 (1998).
[21] W. Brenig, Phys. Rev. B **56**, 14 441 (1997).
[22] H. T. Wang, H. Q. Lin, and J. L. Shen, Phys. Rev. B **61**, 4019 (2000).
[23] Only the case of $\lambda>1$ occurs in physically relevant solutions of the MFT.
[24] W. Brenig and K. W. Becker (unpublished).
[25] P. A. Fleury and R. Loudon, Phys. Rev. **166**, 514 (1968).
[26] O. P. Sushkov and V. N. Kotov, Phys. Rev. Lett. **81**, 1941 (1998).
[27] V. N. Kotov, O. P. Sushkov, and R. Eder, Phys. Rev. B **59**, 6266 (1999).
[28] C. Jurecka and W. Brenig, Phys. Rev. B **61**, 14 307 (2000).
[29] S. Trebst, H. Monien, C. J. Hamer, Z. Weihong, and R. R. P. Singh, Phys. Rev. Lett. **85**, 4373 (2000).
[30] In principle two-particle irreducible vertices can be constructed to second order in b from H_2. In the singlet channel, however, because of the symmetries of the spin indices in Eq. (18) with respect to those of the Levi-Civita symbol in H_2 these vanish identically.
[31] Using a different technique an expression very similar to the denominator of Eq. (27) has been obtained in a study of phonon-assisted optical two-triplet absorption on *spin-1/2 two-leg ladders* (Ref. 28). In contrast to the dimerized $S=1$ chain case, however, $q_c=0$ has been found for the ladder in that case. In that work it was predicted that the singlet bound state of the ladder should be observable in optical absorbtion. Recent work has confirmed this prediction (Ref. 32).
[32] M. Windt, M. Grueninger, T. Nunner, C. Knetter, K. Schmidt, G. S. Uhrig, T. Kopp, A. Freimuth, U. Ammerahl, B. Buechner, and A. Revcolevschi, Phys. Rev. Lett. **87**, 127002 (2001).
[33] P. Lemmens, M. Fischer, G. Güntheroth, C. Gros, P. van Dongen, M. Weiden, W. Richter, C. Geibel, and F. Steglich, Phys. Rev. B **55**, 15 076 (1997).
[34] P. Lemmens, M. Fischer, G. Els, G. Güntherodt, A. S. Mishchenko, M. Weiden, R. Hauptmann, C. Geibel, and F. Steglich, Phys. Rev. B **58**, 14 159 (1998).
[35] P. Lemmens, M. Grove, M. Fischer, G. Güntherodt, V. N. Kotov, H. Kageyama, K. Onizuka, and Y. Ueda, Phys. Rev. Lett. **85**, 2605 (2000).